PREPARATION OF NANOCRYSTALS AND CHITIN MICROFIBRILS

Dorota Biniaś [a, *], Włodzimierz Biniaś [b]

University of Bielsko-Biała, Faculty of Materials, Civil and Environmental Engineering, 43-309 Bielsko-Biała, ul. Willowa 2, Poland
[a] - ORCID: 0000-0002-2548-1774; [b] - ORCID: 0000-0002-7260-7739

** corresponding author: dbinias@ath.bielsko.pl*

Abstract

Chitin nanocrystals and microfibrils were prepared based on the strong acid hydrolysis method. The change in the molecular structure was studied by Fourier-transform infrared and Raman spectroscopy. The surface morphology of chitin materials was observed using scanning electron and optical microscopy. The separation of nano-crystals and microfibril crystalline regions from native chitin may increase the scope of its application for the creation of bioactive composites and scaffolds for tissue culture. As a result of the conducted experimental work, it was possible to loosen the amorphous areas and partially separate nano-crystals and chitin microfibrils. Stable aqueous suspensions of chitin nano-crystals and microfibrils were obtained, which can be used for further experimental work.

Keywords: *nano-crystals chitin, microfibrils chitin, acid hydrolysis, ultrasonic treatment*

Received: 28.02.2022
Accepted: 18.05.2022

1. Introduction

Chitin is one of the most abundant semicrystalline polysaccharides in nature, second only to cellulose. It can be easily extracted from shellfish, fungi, and insects [1]. In general, chitin exists in nature as ordered crystalline microfibrils in the cell wall of fungi and in the exoskeletons of shrimp, crabs, and crustaceans [2]. Natural chitin has three different crystalline isomorphs: the α, β, and γ forms [3]. Due to the ordered, highly crystalline structure, chitin chains tend to connect through hydrogen bonds as well as van der Waals forces that form the microfibre structure. In native chitin, the ordered regions form microfibrils, which consist of nanofibrils embedded in a protein matrix [4]. However, it is generally difficult to convert chitin into individual chitin fibres with a uniform width dispersed in water at the nanofibril level because the chitin fibrils are tightly bound to each other through hydrogen bonds [5]. Chitin nanocrystals (ChiNCs) and chitin nanofibrils (ChiNFs) are the main nanomaterials derived from the pure chitin biopolymer. Acid hydrolysis and mechanical disintegration are the most conventional methods used to prepare ChiNCs and ChiNFs, respectively [6]. ChiNCs obtained by removing the amorphous domain of chitin are natural nanomaterials with a needle shape. They display several advantages including a high aspect ratio, a high specific surface area, a high longitudinal modulus, and a large number of surface functional groups [7-10]. Such chitin nanomaterials can be applied to food, packaging, preparation of water purification membranes, tissue engineering, regenerative medicine, and wound dressing [11-15]. They have also been utilised in electrospinning [16, 17].

2. Materials and Methods

2.1. Materials

Chitin from shrimp shells, practical grade powder $(C_8H_{13}NO_5)_n$, was purchased from Sigma-Aldrich (Poznan, Poland) (C-7170) [1398-61-4] (molecular weight [MW] of 400 kDa, degree of deacetylation [DD] of 3%); 85 wt% phosphoric acid (H_3PO_4) was purchased from CHEMPUR (Piekary Slaskie, Poland) and potassium hydroxide (KOH) and acetone (C_3H_6O) were purchased from Avantor Performance Materials Poland S.A., (Gliwice, Poland). Distilled water was used throughout the experiments unless otherwise specified. All other materials used were of analytical grade.

2.2 Methods

2.2.1. Extraction of Amorphous Chitin by Acid Treatment

The krill chitin used in this research is characterised by a high degree of crystallinity (>80%). High-temperature acid hydrolysis was used to extract amorphous fractions. For this endeavour, commercial shrimp chitin was mechanically milled in a grinder. Figure 1 shows digital images of the samples obtained before and after mechanical grinding.

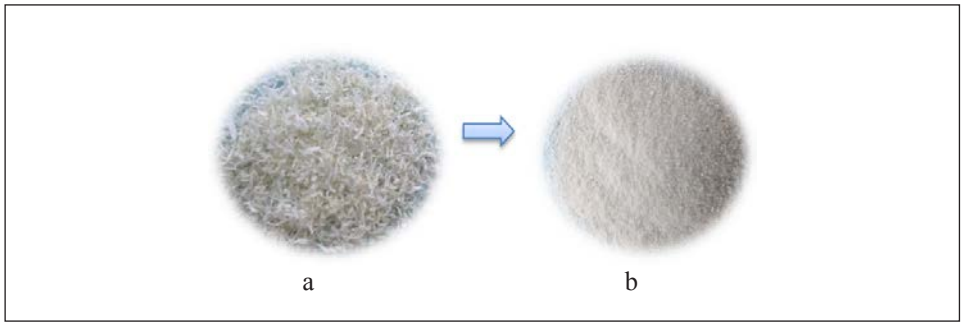

Figure 1. Digital images of the chitin before (a) and after (b) mechanical grinding.

Polarised light microscopy with Nomarski contrast was used to analyse changes in the morphological structure of chitin. Before hydrolysis, chitin samples were taken from the suspension and placed on a glass slide (Figure 2).

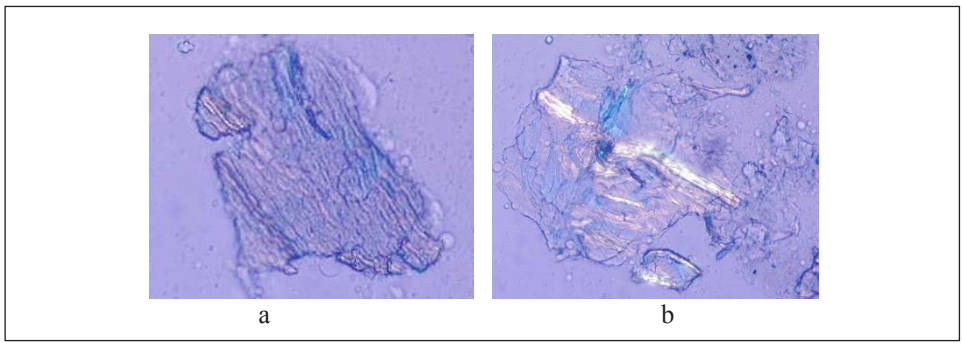

Figure 2. Optical micrographs of chitin samples before hydrolysis in phosphoric acid.

The next step was treatment of chitin with 4 M H_3PO_4 at 95°C. The pH of 4 M H_3PO_4 is 0.89. However, this value changes with the time of interaction with chitin and increases to over 1.2. Chitin samples were taken during acid hydrolysis (at 1, 2, and 3 h) to observe changes in the morphological structure using polarised light microscopy. After hydrolysis, the samples were rinsed with distilled water, followed by treatment with 4 M KOH to neutralise the acid. Subsequently, the chitin was rinsed several times with distilled water to rinse the formed salts and ensure an appropriate pH of 6, and the chitin was filtered off in a Büchner funnel.

2.2.2. Ultrasound Treatment of Chitin

After hydrolysis, chitin was dispersed in distilled water and placed in an ice bath to cool it during sonication. Ultrasound treatment was performed using a Vibra-Cell model VC 505 sonicator from Sonics & Materials Inc. (Newtown, CT, USA). The process parameters were: CV 334 head, standard 13 mm (1/2") diameter, pulse 10/5, amplitude 40%, frequency 20 kHz, and power 500 W. Figure 3 shows a schematic diagram of the apparatus used for chitin sonication.

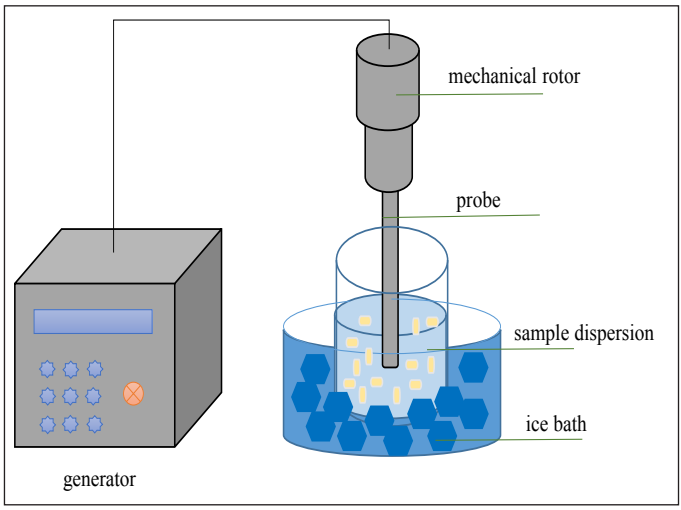

Figure 3. Schematic representation of ultrasonic homogenisation.

The sonication lasted for 30 min, divided into three cycles of 10 min. A sample of the chitin suspension was collected after each cycle to measure visible transmission. Digital images of the chitin suspension at the different stages of sonication are shown in Figure 4.

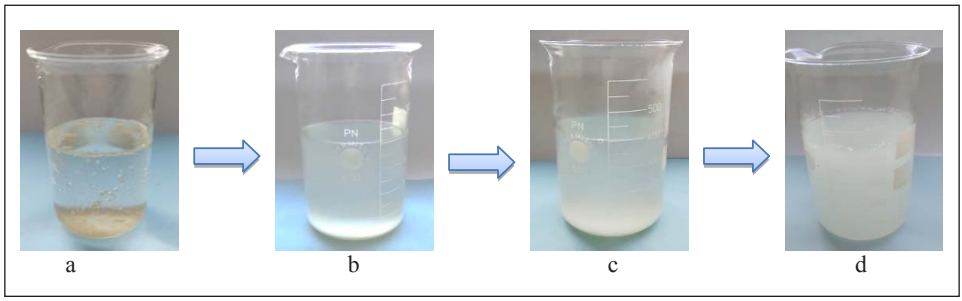

Figure 4. Digital images of the chitin suspension before sonication (a) and after 10 min (b), 20 min (c), and 30 min (d) of sonication.

2.2.3. Characterisation of Chitin Materials

2.2.2.1. Fourier-Transform Infrared (FTIR) Spectroscopy

FTIR spectroscopy was performed using a Nicolet 6700 spectrometer equipped with an EasiDiff diffusion accessory (Thermo Fisher Scientific, Waltham, MA, USA). The spectral region was as follows: 4000-400 cm^{-1}, resolution 8 cm^{-1}, number of scans 128, and deuterated triglycine sulphate detector. Data collection and post-processing were performed using OMNIC software (v. 9.0, Thermo Scientific Electron Corp.). Each spectrum was analysed with the use of a linear baseline and processed with the smoothing function.

2.2.2.2. Ultraviolet-visible (UV-Vis) Spectroscopy

The UV-Vis spectra were obtained with an Evolution™ 300 (Thermo Scientific). The measurements were made for chitin suspensions in aqueous solutions obtained after the sonication steps; the background was a sample with distilled water. The measurement range was 900-190 nm. The spectra were processed using the VISIONPro software (Thermo Scientific).

2.2.2. Analysis of Morphology

2.2.2.1. Scanning Electron Microscopy (SEM)

The morphology and the structure of the chitin were observed by SEM with a JSM 5500 LV (Tokyo, Japan), equipped with a Wolfram cathode at an accelerating voltage of 10 kV. Before SEM observation, the samples were sputter-coated with gold.

2.2.2.2. Optical Microscopy

The morphologies of the obtained materials before and after hydrolysis were observed using a DIAPAN optical microscope (Reichert, Vienna, Austria) coupled with a ARTCAM CCD camera (Olympus, Tokyo, Japan), using MOTIC IMAGES PLUS 2.0 software.

3. Results and Discussion

The FTIR spectra of chitin from shrimp shells and chitin after hydrolysis and sonification are shown in Figures 5 and 6. The major spectral peaks observed in the FTIR as well as the peak assignments are shown in Table 1 [18-23].

Table 1. Band assignments of the Fourier-transform infrared spectrum of chitin [18-23].

Functional group and vibration modes	Classification	Wavenumber (cm^{-1})
O-H hydroxyl stretching	-	3600-3000
N-H stretching	Amide	3250-3100
Asymmetric C-H stretching	Aliphatic compounds	2960-2920
Symmetric C-H stretching	Aliphatic compounds	2880-2850
C=O stretching C=O stretching	Amide I Amide I	1680-1640 1625-1620
O=H bending	-	1635
N-H in-plane C-N stretching	Amide II	1570-1540
C-H bending CH_3 deformation	-	1450-1430
Symmetric C-H bending Symmetric CH_3 deformation	-	1380-1375
CH_2 wagging	Amide III, components of proteins	1315-1308
Asymmetric C-O-C stretch in phase	Saccharide rings	1155-1153
Asymmetric C-O stretch in phase ring, stretching mode		1115-1110
Asymmetric C-O-C stretching in-phase ring	Saccharide rings	1075-1050
Asymmetric C-O stretch in phase ring		1045-1000
C-H wagging	Along chain	950
C-H ring stretching	Saccharide rings	895-877

Absorption bands at 2960 cm^{-1} and 2885 cm^{-1} are due to asymmetric and symmetric C-H stretching. The chitin samples can be distinguished by FTIR spectroscopy through the vibration modes of amide I in the spectral region of 1675-1630 cm^{-1}. In the FTIR spectra of chitin, there are two absorption bands at about 1650 and 1620 cm^{-1} (C=O stretching). The amide II band at 1568 cm^{-1} is characteristic of chitin. Peaks at 1382 and 1320 cm^{-1} may be assigned to O-H deformation of -CH_2-OH and -CH-OH, although they overlap with -CH_3 deformation and -CH_2 wagging [9]. The band at 1320 cm^{-1} corresponds to the C-N bond, and the peak at 1163 cm^{-1} is asymmetric stretching of the bridge oxygen (C-O-C). There is a prominent band at around 1125 cm^{-1} corresponding to asymmetric C-O-C and anhydroglucose ring asymmetric stretching. The bands at 1088 and 1040 cm^{-1} are caused by asymmetric stretching of both C-O-C and pyranose groups [18].

As a result of sonication, there is a characteristic shift of practically all bands in the 1800-1000 cm^{-1} range towards higher wavenumbers. Such a phenomenon can be observed in the case of dissociation of hydrogen interactions, which leads to their weakening

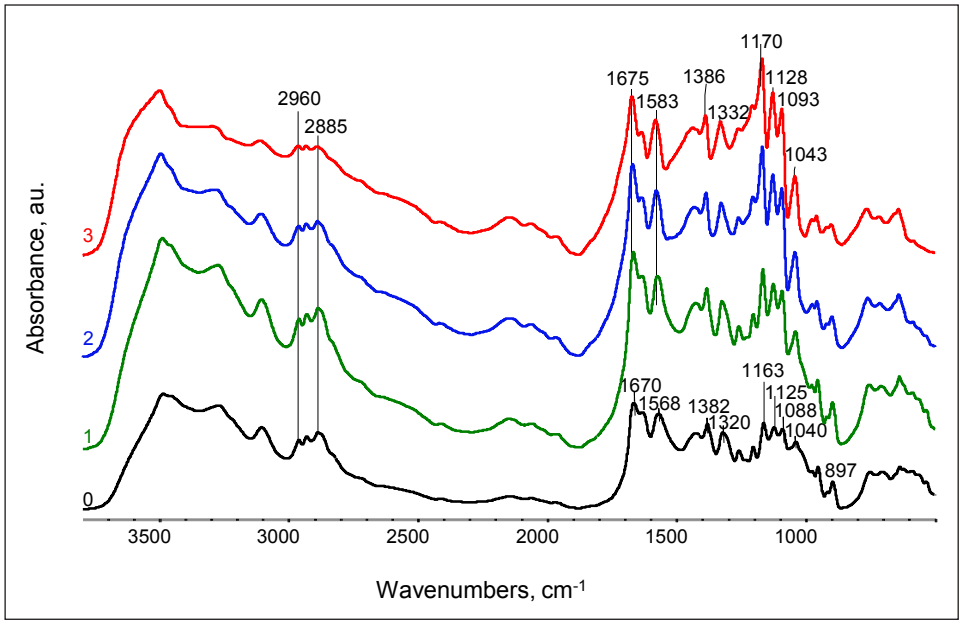

Figure 5. Fourier-transform infrared spectra of native chitin from shrimp shells (0) and chitin after hydrolysis and sonication (1 = 1 h, 2 = 2 h, and 3 = 3 h).

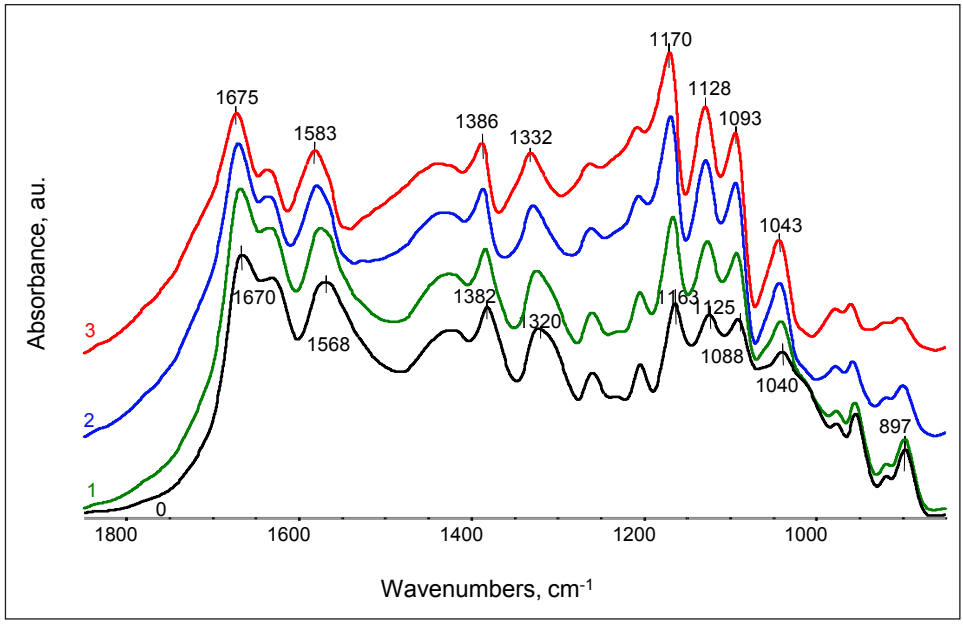

Figure 6. Fourier-transform infrared spectra of native chitin from shrimp shells (0) and chitin after hydrolysis and sonication (1 = 1 h, 2 = 2 h, and 3 = 3 h).

or breaking. In the case of strong mechanical interactions that take place during sonication, the intermolecular interactions between individual chitin groups are relaxed. On the obtained spectra, there is sharpening of individual bands, which may confirm the formation of molecular structures with the same oscillation parameters of the groups corresponding to the ordered regions. This may be due to the relaxation or partial decomposition of amorphous regions and obtaining a material with the same ordered molecular structure.

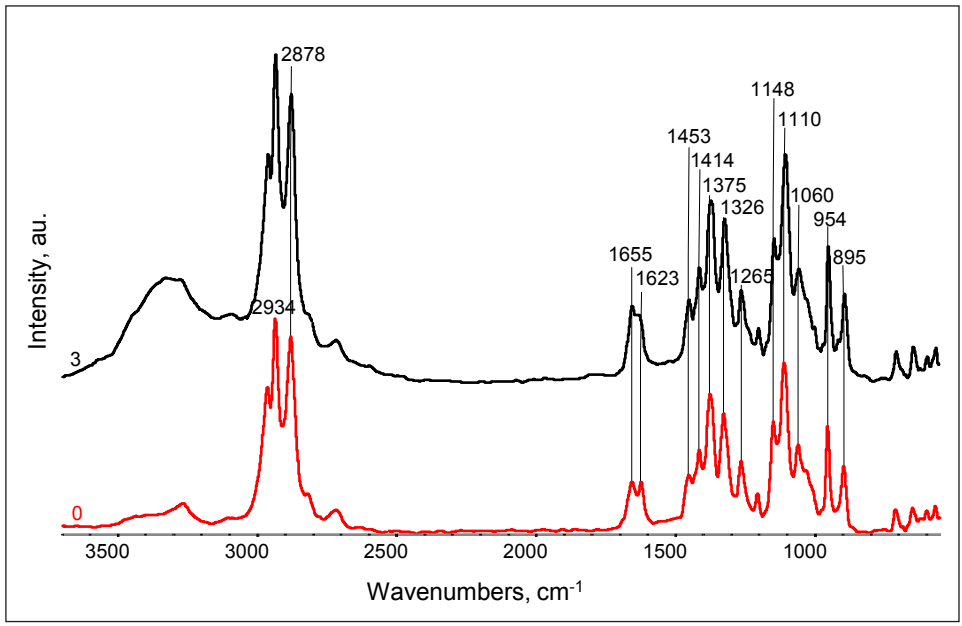

Figure 7. Fourier-transform Raman spectra of native chitin from shrimp shells (0) and chitin after the process of hydrolysis and sonication (3 = 3 h of hydrolysis and sonication).

Analysis of the Raman spectra before and after sonication shows very slight differences in the structure of symmetrical groups along the polymer chains (Figure 7). This effect can be explained by the behaviour of the chain structure and its conformation. Compared with the FTIR spectra, this indicates a loosening of the amorphous structure and the maintenance of ordered areas. Therefore, it confirms the breakdown of chitin into individual crystal fibrils.

Figure 8 shows scanning electron micrographs of the native chitin from shrimp after mechanical grinding.

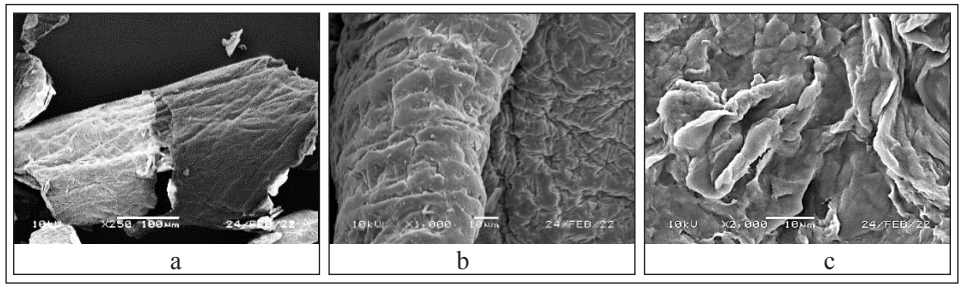

Figure 8. Scanning electron micrographs of the chitin from shrimp with different magnification. The scale bar is 100 μm (a), 10 μm (b), and 10 μm (c).

Figures 9, 10, and 11 show micrographs obtained by polarised light microscopy 1, 2, and 3 h of hydrolysis in H_3PO_4, respectively.

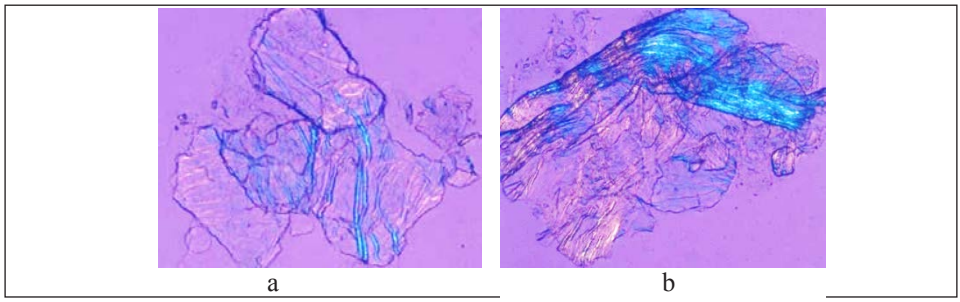

Figure 9. Polarised light micrographs of chitin samples after 1 h of hydrolysis in phosphoric acid.

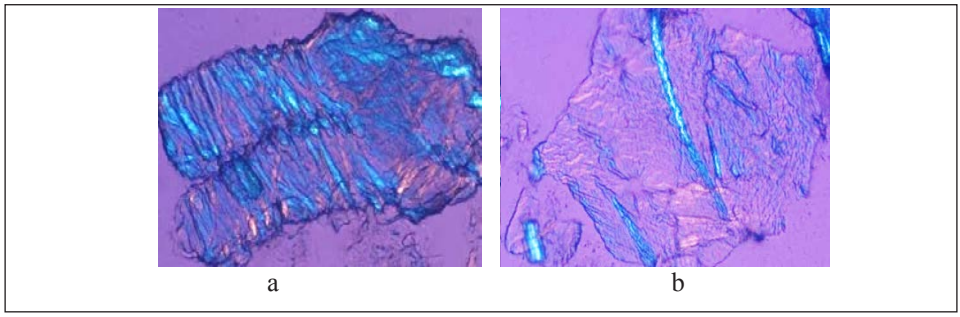

Figure 10. Polarised light micrographs of chitin samples after 2 h of hydrolysis in phosphoric acid.

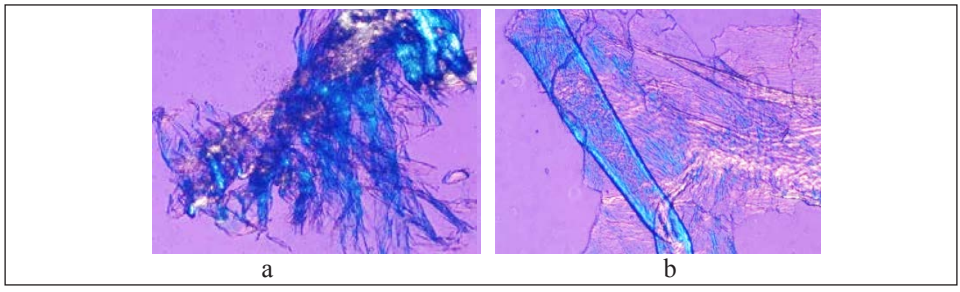

Figure 11. Polarised light micrographs of chitin samples after 3 h of hydrolysis in phosphoric acid.

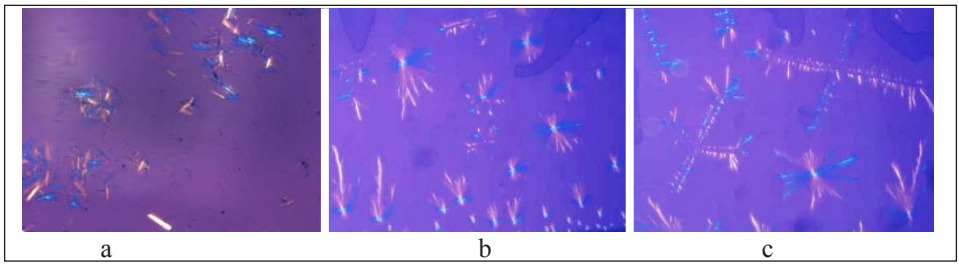

Figure 11. Polarised light micrographs of the chitin samples after hydrolysis and sonication.

Analysis of microscopic photos in polarised light with the use of Nomarski contrast, taken at different stages of hydrolysis and after sonication, indicates a gradual selective separation of the chitin structure during processing. In the final step of the process (Figure 12), the arrangement of the isolated fibrils in the crystalline regions is apparent. Fibrils, depending on the mutual position of fibrils and the plane of light polarisation, are light or dark objects, whereas the amorphous material is transparent.

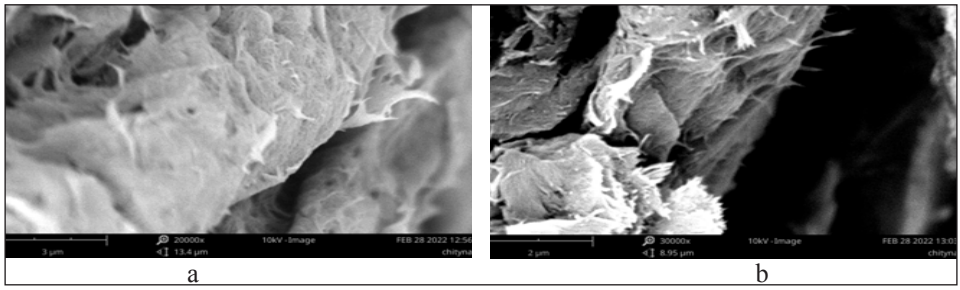

a b

Figure 13. Scanning electron micrographs of the chitin samples after hydrolysis and sonication (3 h). The scale bar is 3 μm (a) and 2 μm (b).

In the scanning electron micrographs of chitin, after the longest time of hydrolysis and sonication (Figure 13), there are isolated systems arranged in the form of fibrils clusters.

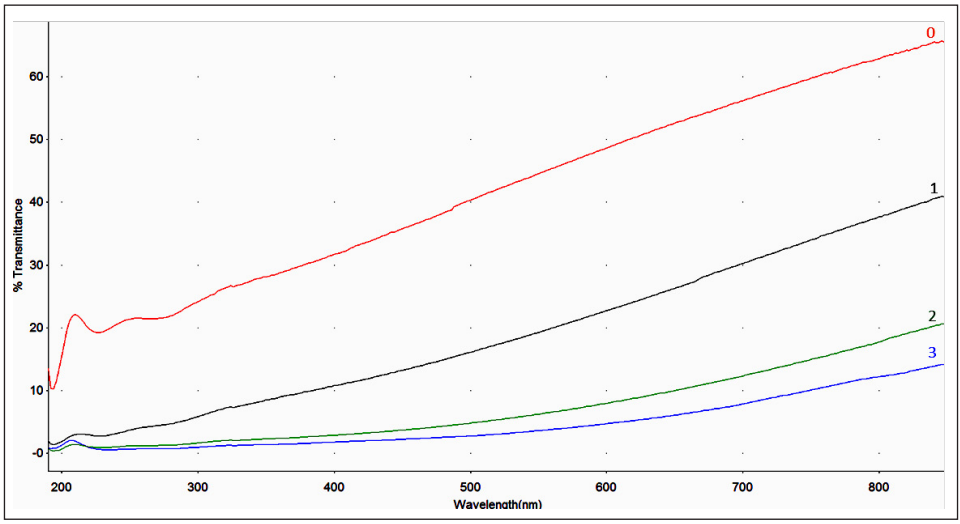

Figure 13. Ultraviolet-visible spectra of the chitin suspension before sonication (0) and after the individual sonication steps (1 = after 1 h, 2 = after 2 h, and 3 = after 3 h of hydrolysis and sonication).

To determine the degree of fragmentation of chitin fragments, the degree of light scattering in the visible range by the sonicated suspensions was determined (Figure 14). There was a decrease in transmission for individual samples during hydrolysis and sonication, which confirms that light scattering increases with time. However, hydrolysis and sonication did not cause the same reduction in transmission. It can be interpreted as

a phenomenon with decreasing breakdown of particles into crystalline regions after the same hydrolysis time. Further hydrolysis and sonication can lead to a suspension with only crystalline structures. However, it cannot be ruled out that further hydrolysis would affect the crystalline regions and the suspension would be more transparent. However, this eventuality requires confirmation by additional research.

4. Conclusions

The gradual hydrolysis of native chitin combined with the mechanical effect of the sonicator probe enables the separation of microfibre-structured areas from the semicrystalline structure. The tests of the separation products revealed significant loosening of the chitin structure through the hydrolysis of amorphous areas more easily accessible to the acid. Subsequently, the mechanical effects caused by the vibrations of the sonicator probe resulted in separation of chitin microfibrils. The process conditions did not noticeably affect the conformational structure of the chitin molecules in the ordered regions. Combined physicochemical and mechanical processing produced a form of chitin that could be useful for the preparation of bioactive composites or scaffolds for tissue engineering.

5. References

[1] Kumar MR; (1999) Chitin and chitosan fibers: a review. Bull Mater Sci 22(5), 905.
[2] Yan N, Chen X; (2015) Don't waste seafood waste. Nature 524, 155-157. doi:10.1038/524155a.
[3] Zeng J-B, He Y-S, Li S-L, Wang Y-Z; (2012) Chitin whiskers: an overview. Biomacromolecules 13(1), 1-11. **DOI**:10.1021/acsami.0c12176
[4] Chen P-Y, Lin AY-M, McKittrick J, Meyers MA; (2008) Structure and mechanical properties of crab exoskeletons. Acta Biomater 4(3), 587-596
[5] Shams MI, Ifuku S, Nogi M, Oku T, Yano H; (2011) Fabrication of optically transparent chitin nanocomposites. Appl Phys A 102 (2), 325-331.
[6] Larbi F, García A, del Valle LJ, Hamou A, Puiggalí J, Belgacem N, Bras J; (2018) Comparison of nanocrystals and nanofibers produced from shrimp shell α-chitin: from energy production to material cytotoxicity and Pickering emulsion properties. Carbohydr Polym 196, 385–397. **DOI**:10.1016/j.carbpol.2018.04.094
[7] Zhao H-P, Feng X-Q, Gao H; (2007) Ultrasonic technique for extracting nanofibers from nature materials. Appl Phys Lett 90(7), 073112.
[8] Ou X, Yang X, Zheng J, Liu M.; (2019) Free-standing graphene oxide–chitin nanocrystal composite membrane for dye adsorption and oil/water separation. ACS Sustainable Chem Eng 7(15), 13379-13790. **DOI**:10.1021/acssuschemeng.9b02619
[9] Ou X, Cai J, Tian J, Luo B, Liu M.; (2020) Superamphiphobic surfaces with self-cleaning and antifouling properties by functionalized chitin nanocrystals. ACS Sustainable Chem Eng 8(17), 6690-6699. **DOI**:10.1021/acssuschemeng.0c00340
[10] Zhang M, Li Y, Wang W, Yang Y, Shi X, Sun M, Li Y; (2020) Comparison of physicochemical and rheology properties of Shiitake stipes-derived chitin nanocrystals and nanofibers. Carbohydr Polym 244, 116468. **DOI**:10.1016/j.carbpol.2020.116468
[11] Salaberria AM, Labidi J, Fernandes SCM; (2014) Chitin nanocrystals and nanofibers as nano-sized fillers into thermoplastic starch-based biocomposites processed by melt-mixing. Chem Eng J 256(15), 356-364
[12] Shankar S, Reddy JP, Rhim JW, Kim HY; (2015) Preparation, characterization, and antimicrobial activity of chitin nanofibrils reinforced carrageenan nanocomposite films. Carbohydr Polym 117, 468-475.

[13] Shankar S, Oun AA, Rhim JW; (2018) Preparation of antimicrobial hybrid nanomaterials using regenerated cellulose and metallic nanoparticles. Int J Biol Macromol 10(7), 17-27.
[14] Wu C, Li Y, Sun J, Lu Y, Tong C, Wang, L, Yan Z; (2020) Novel konjac glucomannan films with oxidized chitin nanocrystals immobilized red cabbage anthocyanins for intelligent food packaging. Food Hydrocolloids 98. **DOI**:10.1016/j.foodhyd.2019.105245
[15] Zhou J, Zhou Q, Yan M; (2014) Glycan-functionalized fluorescent chitin nanocrystals for biorecognition applications. Bioconjugate Chem 25, 640-643.
[16] Gopi S, Balakrishnan P, Pius A, Thomas S; (2017) Chitin nanowhisker (ChNW) - functionalized electrospun PVDF membrane for enhanced removal of Indigo carmine. Carbohydr Polym 165, 115-122.
[17] Naseri N, Algan C, Jacobs V, John M, Oksman K, Mathew AP; (2014) Electrospun chitosan-based nanocomposite mats reinforced with chitin nanocrystals for wound dressing. Carbohy Polym 109, 7-15. **DOI**:10.1016/j.carbpol.2014. 03.031
[18] Biniaś D, Biniaś W, Janicki J; (2018) Formation of fibers and microspheres from chitin solution. Prog Chem Appl Chitin Deriv 23, 25-32, DOI:10.15259/PCACD.23.002
[19] Cárdenas G, Cabrera G, Taboada E, Miranda SP; (2004) Chitin characterization by SEM, FTIR, XRD, and 13C cross polarization/mass angle spinning NMR. J Appl Polym Sci 93(4), 1876-1885.
[20] Kaya M, Baran T, Mentes A, Asaroglu M, Sezen G, Tozak KO; (2014) Extraction and characterization of a-chitin and chitosan from six different aquatic invertebrates. Food Biophys 9(2), 45-157.
[21] Chaussard G, Domard A; (2004) New aspects of the extraction of chitin from squid pens, Biomacromolecules 5(2), 559-564.
[22] Kaya M, Baran T, Erdoğan S, Menteş A, Özüsağlam MA, Çakmak YS; (2014) Physicochemical comparison of chitin and chitosan obtained from larvae and adult Colorado potato beetle (*Leptinotarsa decemlineata*). Mater Sci Eng C 45, 72-81. **DOI**:10.1016/j.msec.2014.09.004
[23] Kumirska J, Czerwicka M, Kaczyński Z, Bychowska A, Brzozowski K, Thöming J, Stepnowski P; (2010) Application of spectroscopic methods for structural analysis of chitin and chitosan. Marine Drugs 8(5), 1567-1636. **DOI**:10.3390/md8051567